Modeling of Hydrogenation of Maleic Acid in a Bubble-Column Slurry Reactor

Nakul N. Thakar, Rengaswamy Jaganathan, and Raghunath V. Chaudhari
Homogeneous Catalysis Division, National Chemical Laboratory, Pune 411008, India

Patrick L. Mills
DuPont Company, Experimental Station, Wilmington, DE 19880

A bubble-column slurry-reactor model has been developed for the hydrogenation of aqueous maleic acid (MAC) to tetrahydrofuran (THF). This particular reaction system has recent commercial relevance and represents a case where complex multistep catalytic hydrogenation reactions are conducted at high pressure (>15 MPa) and high temperature (>240°C). It also has additional complexities associated with the reaction chemistry, since the THF reaction product is volatile and the reaction is highly exothermic. The proposed model is derived using the mixing cell approach and incorporates the contributions of gas–liquid and liquid–solid mass transfer, intraparticle diffusion effects, product volatility, heat effects, and complex multistep reaction kinetics. The effect of gas and liquid velocities, catalyst loading, inlet maleic acid concentration, and temperature on the conversion, selectivity, temperature rise, and productivity of the desired products (THF and γ-butyrolactone (GBL)) is also discussed. Since the reaction step involving the hydrogenation of GBL to THF is relatively slow, severe operating conditions are necessary to achieve high THF selectivity. The distribution pattern of THF in the gas and liquid phases is also discussed. The model proposed could be useful for simulation of existing pilot- or industrial-scale reactors, as well as the design and scale-up of new reactors for this particular reaction or one that has similar characteristics.

Introduction

Bubble-column slurry reactors (BCSRs), which involve contacting of gaseous and liquid reactants in the presence of suspended solid catalyst particles, are extensively used in several industrial chemical and petroleum-refining processes. The design and scale-up of these reactors is of considerable interest, since a number of both fundamental and practical issues can be defined that introduce uncertainties in the prediction of reactor performance. Important developments on the reaction engineering analysis of BCSRs were reviewed in earlier work by Shah (1979), Ramachandran and Chaudhari (1983), and Deckwer (1992). More recent reviews have been provided by Saxena (1995), Krishna (2000), and in the monograph of Schumpe and Nigam (1996). Some examples of the commercial applications of BCSRs include Fischer-Tropsch synthesis (Bukur, 1983; Mills et al., 1996; Krishna et al., 1998, 2001), hydrogenation of adiponitrile (Mathieu et al., 1992), hydrogenation of oils (Bern et al., 1975), and several unsaturated compounds.

In the applications just cited, either a semibatch or continuous mode is utilized, or in some cases, a continuous flow with recycle operation is followed. The overall performance of such reactors depends on the specific reaction kinetics, external and intraparticle mass transfer, gas- and liquid-phase mixing parameters, hydrodynamics, solid catalyst distribution and thermal energy management. While the analysis of multiphase catalytic reactors has been well developed from a theoretical perspective for simple reaction schemes, information on the analysis of reactor performance behavior for industrially useful processes in BCSRs is very limited. In previous

Correspondence concerning this article should be addressed to R. V. Chaudhari.

work on the modeling of BCSRs, detailed consideration has been given to hydrodynamic modeling, particularly CFD modeling (Krishna and Maretto, 1998; Krishna et al., 2001), evaluation of mixing (Govindarao and Chidambaram, 1983), and mass-transfer parameters (Kawakami et al., 1981; Dassori, 1998). Although reactor performance models have been proposed for several reactions, such as the Fischer-Tropsch synthesis (Mills et al., 1996; Krishna and Maretto, 1998; Krishna et al., 2001), hydrogenation of glucose (Brahme et al., 1984), and the hydrogenation of butynediol (Jaganathan et al., 1987), in most of these cases, only single reactions with simplified kinetics have been considered. Industrial BCSRs typically involve complex multistep catalytic reactions with complexities such as nonlinear kinetics, catalyst deactivation, exothermic reactions, volatile reactants and products, and nonuniform distribution of catalyst particles. One such recent commercial example is the hydrogenation of aqueous MAC to THF as the desired product. The direct hydrogenation of MAC to THF is considered a major advancement in chemical technology for THF production when compared to the conventional processes, and it has been recently commercialized by DuPont (Stadig, 1992). This reaction is the second step of a two-step process in which butane is oxidized to maleic anhydride (MAN) in the first reaction step using a circulating solids reactor system. The crude MAN is then absorbed in water to produce a crude MAC stream by hydrolysis, which is then fed to a BCSR. Some of the novel features of this process include specially designed bimetallic catalysts, such as 1% Pd/4% Re-on-carbon (Ernst and Michel, 1992), and 1% Ru/4% Re-on-carbon (Schwartz, 1995), as well as a novel reactor design that operates at a high temperature (200°C to 250°C) and pressure (14 MPa to 20 MPa) with a continuous removal of the volatile THF product.

The objective of this article is to develop a BCSR model for the hydrogenation of MAC to THF for predictions of conversion, selectivity, temperature rise, and productivity of THF in the reactor for a given set of input parameters. Rather than use a detailed CFD model whose parameters are the subject of much debate (Harris et al., 1996), a mixing-cell model is utilized that incorporates the contributions of reaction kinetics, gas–liquid and liquid–solid mass transfer, intraparticle diffusion effects, overall heat transfer, and volatility effects associated with the aqueous reaction mixture. Also, the existing CFD codes are not adequate to describe the churn turbulent behavior in a reactor with multiport sparger. The model presented here is useful for developing insight into the effects of various operating parameters on the overall reactor performance. It also may be utilized for guiding the design and scale-up of such systems from lab-scale and pilot-scale data. Even though a large amount of information is available in the literature on mixing in bubble columns, these are mainly for air–water systems under ambient conditions. Only a limited amount of data is available for reaction systems under high temperatures and pressures.

Reactor Model Development

The generic reactor models previously proposed for BCSRs (Ramachandran and Smith, 1979; Kawakami et al., 1981; Jaganathan et al., 1987; Kralik et al., 1990) could not be used for modeling the performance of a BCSR for the hydrogenation of MAC to THF, since these do not account for the various complexities of this system. In the following section, a detailed analysis of a BCSR model has been presented using a mixing-cell approach. This model incorporates the complexities of reaction kinetics coupled with external and intraparticle mass transfer, thermal effects, variable gas velocity, and vaporization of the reaction media/solvent (water) and the major product THF. In this process, THF is the desired product, while γ-butyrolactone (GBL) and succinic acid (SAC) are the primary intermediates. A small amount (< 5 wt %) of *n*-butanol is also present as a side product. Since THF is volatile (BP = 67°C at 1 bar), under reaction conditions, it can be continuously removed as a vapor in the exit gas stream, while the liquid phase intermediates and products remain largely confined to the liquid phase. The continuous removal of THF simplifies the process and also prevents further hydrogenation of THF to *n*-butanol.

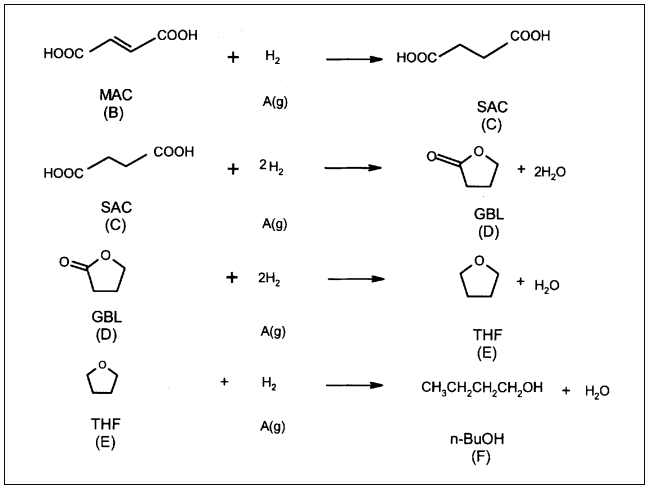

Figure 1. Reaction scheme for hydrogenation of maleic acid.

Intrinsic kinetics

The intrinsic kinetics for the hydrogenation of MAC to THF with a Ru–Re/C catalyst have been recently studied by Chaudhari et al. (2003) using a batch-slurry reactor from 503 K to 543 K, 14 MPa to 20 MPa, and catalyst loading from 20 kg/m^3 to 100 kg/m^3. Based on this work, the reaction network can be described as shown in Figure 1. The following types of Langmuir-Hinshelwood (L-H) rate equations have been found to adequately describe the individual reaction steps involved, where the subscripts 1–4 refer to MAC, SAC, GBL, and THF, respectively.

$$r_1 = \frac{wk_1 A_s B_s}{(1 + K_A A_s + K_B B_s + K_C C_s + K_D D_s)^2} \quad (1)$$

$$r_2 = \frac{wk_2 A_s C_s}{(1 + K_A A_s + K_B B_s + K_C C_s + K_D D_s)^2} \quad (2)$$

$$r_3 = \frac{wk_3 A_s D_s}{(1 + K_A A_s + K_B B_s + K_C C_s + K_D D_s)^2} \quad (3)$$

Table 1. Kinetic Rate Equation Parameters

Temperature (K)	$k_1 \times 10^5$	$k_2 \times 10^6$	$k_3 \times 10^6$	$k_4 \times 10^7$	K_A	K_B	K_C	K_D
503	1.251	4.102	2.098	2.841	0.201	0.989	0.508	0.051
523	9.584	8.881	2.912	5.345	0.304	1.513	0.901	0.131
543	25.281	28.013	9.452	7.334	0.499	2.519	1.981	0.314

Units of k_j: (m^3/kmol)(m^3/kg/s); units of K_A, K_B, K_C, K_D: (m^3/kmol).

$$r_4 = \frac{wk_4 A_s E_s}{(1 + K_A A_s + K_B B_s + K_C C_s + K_D D_s)^2} \tag{4}$$

By combining Eqs. 1–4, it can be shown that the overall rate of hydrogenation can be given as

$$R_A = \frac{\eta_c w(k_1 B_s + k_2 C_s + k_3 D_s + k_4 E_s) A_s}{(1 + K_A A_s + K_B B_s + K_C C_s + K_D D_s)^2} \tag{5}$$

where η_c denotes the catalyst effectiveness factor.

In Eqs. 1–5, A_s represents the concentration of dissolved hydrogen on the catalyst surface. The parameters B_s, C_s, D_s, and E_s represent the concentrations of MAC, SAC, GBL, and THF, respectively, on the catalyst surface. Definitions for the remaining kinetic rate equation variables appear in the Notation Section. The values for the rate and adsorption equilibrium constants that were obtained by kinetic parameter estimation from the batch slurry reactor data for Eqs. 1–4 are listed in Table 1 (Chaudhari et al., 2002). The activation energies for the rate constants k_1, k_2, k_3, and k_4 are shown in Table 2. The adsorption parameters increase with temperature, indicating an endothermic process. This observation, though uncommon, also has been reported previously in the literature (Broderic and Gates, 1981) for liquid-phase hydrogenation reactions.

Bubble-Column-Slurry-Reactor Model

Assumptions. Ramachandran and Chaudhari (1983) have systematically described the modeling of continuous three-phase reactors for various flow patterns of gas and liquid and various reaction schemes. Since the problem considered here involves complex multistep reactions coupled with mass transfer, heat effects, and solvent/product volatility, a mixing-cell approach proposed earlier by Ramachandran and Smith (1979), Brahme et al. (1984), and Jaganathan et al. (1987) was followed. In the development of the reactor model, the following assumptions were made:

(1) The BCSR is visualized as consisting of N cells of stirred tanks in series where the liquid is completely back mixed and gas is in plug flow in each cell. Thus, for $N \to \infty$, plug flow will prevail, while for $N = 1$, the reactor performance will be equal to a back mixed slurry reactor. Intermediate values of N will describe liquid-phase flow patterns between these two extremes.

(2) Gas–liquid, liquid–solid, and intraparticle mass-transfer resistances have been incorporated for hydrogen. For the nonvolatile liquid components, the intraparticle diffusion has been assumed to be negligible, since the concentration of these are expected to be several orders of magnitude higher than that of dissolved hydrogen in the reactor.

(3) The catalyst particles are assumed to be dispersed uniformly throughout the reactor. To verify this assumption, the approach of Kato et al. (1972) was followed. It was found that the catalyst concentration at the end of the reactor was 99.83% of the average catalyst loading.

(4) Interphase and intraparticle heat transfer are negligible, but overall heat transfer from the bulk liquid phase to the reactor wall has been accounted for. To verify the first assumption, the criteria proposed by Mears (1971) were used.

(5) The volatility of THF, which is the desired product, and solvent water has been incorporated, including the change in gas velocity due to product stripping and its effect on other parameters.

Model Equations. The mass- and energy-balance equations for various species in a BCSR are summarized below. Here, the variables A_j, B_j, C_j, D_j, E_j, and F_j represent the concentration of the gas- and liquid-phase species, leaving the jth cell while those entering the jth cell are represented by A_{j-1}, B_{j-1}, C_{j-1}, D_{j-1}, E_{j-1}, and F_{j-1}. An analogous approach is used for the cell temperatures. The mass balance for the various species exiting the jth cell are given below in the dimensionless form. The dimensionless parameters used in these equations are defined in Table 3.

For Species A (Hydrogen). In the gas phase

$$-\frac{da_{g_j}}{dz} = \alpha_A[a_{g_j} - a_{l_j}] \tag{6}$$

In the liquid phase

$$\int_0^1 \alpha_A \beta_A[a_{g_j} - a_{l_j}]\, dz = [a_{l_j} - a_{l_{j-1}}] + \frac{\alpha_s}{N}[a_{l_j} - a_{s_j}] \tag{7}$$

and

$$\alpha_s[a_{l_j} - a_{s_j}] = \alpha_R \eta_c \left[\frac{b_{s_j} + 2k_{21}c_{s_j} + 2k_{31}d_{s_j} + k_{41}e_{s_j}}{(1 + k_a a_{s_j} + k_b b_{s_j} + k_c c_{s_j} + k_d d_{s_j})^2}\right] a_{s_j} \tag{8}$$

For Species B (MAC). In the liquid phase

$$[b_{l_{j-1}} - b_{l_j}] = \frac{\alpha_s}{N}(b_{l_j} - b_{s_j}) \tag{9}$$

Table 2. Activation Energy Parameters

E_1	165 kJ/mol
E_2	108 kJ/mol
E_3	106 kJ/mol
E_4	53.8 kJ/mol

Table 3. Dimensionless Parameters Used in the Model

Mass-transfer parameters	
Gas–liquid mass transfer	$\alpha_A = k_l a_B L/u_g H_A \qquad \alpha_E k_l a_B L/u_g H_E$
Liquid–solid mass transfer	$\alpha_s = k_s a_p L/u_l$
Catalyst effectiveness factor	$\eta_c = \frac{1}{\phi}\left[\coth(3\phi) - \frac{1}{3\phi}\right]$
	$\phi = \phi_0[(b_l + k_{21}c_l + k_{31}d_l + k_{41}e_l)]^{1/2}$
	$\times\left[\ln(1 + k_a a_s + k_b b_l + k_c c_l + k_d d_l) + \frac{(1 + k_b b_l + k_C c_l + k_d d_l)}{(1 + k_a a_s + k_b b_l + k_C c_l + k_d d_l)}\right]^{1/2}$
Thiele parameter	$\phi_0 = \frac{R}{3}\left[\frac{\rho_p k_1 B_{l_1}}{2D_e}\right]$
Heat transfer parameters	
1. Thermicity parameter	$\beta 1 = \frac{-\Delta HrB_{l_1}}{(\rho Cp)_l T_0\left[1 + \frac{u_g(\rho Cp)_g}{u_l(\rho Cp)_l} + \frac{u_s(\rho Cp)_s}{u_l(\rho Cp)_l}\right]}$
2. Bed-to-wall heat transfer	$\beta 2 = \frac{4U_w L/N}{u_l(\rho Cp)_l\left[1 + \frac{u_g(\rho Cp)_g}{u_l(\rho Cp)_l} + \frac{u_s(\rho Cp)_s}{u_l(\rho Cp)_l}\right]}$
3. Evaporation term for solvent	$\beta 3 = \frac{\rho_s \Delta H_s u_{s_i 1}}{u_l(\rho Cp)_l T_0\left[1 + \frac{u_g(\rho Cp)_g}{u_l(\rho Cp)_l} + \frac{u_s(\rho Cp)_s}{u_l(\rho Cp)_l}\right]}$
4. Evaporation term for THF	$\beta 4 = \frac{\rho_g \Delta H_{evTHF} u_{g_i 1}}{u_l(\rho Cp)_l T_0\left[1 + \frac{u_g(\rho Cp)_g}{u_l(\rho Cp)_l} + \frac{u_s(\rho Cp)_s}{u_l(\rho Cp)_l}\right]}$
Reaction rate and equilibrium constants	$k_{21} = \frac{k_2}{k_1};\ k_{31} = \frac{k_3}{k_1};\ k_{41} = \frac{k_4}{k_1}$
	$k_a = K_A A_{s_j};\ k_b = K_B B_{s_j};\ k_c = K_C C_{s_j};\ k_d = K_D Ds_j$
	$\alpha_R = \frac{wk_1 B_{l_1} L}{u_l}$

and

$$\alpha_s\left(b_{l_j} - b_{s_j}\right) = \frac{\alpha_R}{q_B}\eta_c\left[\frac{a_{s_j} b_{s_j}}{\left(1 + k_a a_{s_j} + k_b b_{s_j} + k_c c_{s_j} + k_d d_{s_j}\right)^2}\right] \tag{10}$$

For Species C (SAC). In the liquid phase

$$\left[c_{l_j} - c_{l_{j-1}}\right] = \frac{\alpha_s}{N}\left[c_{l_j} - c_{s_j}\right] \tag{11}$$

and

$$\alpha_s\left[c_{l_j} - c_{s_j}\right] = \frac{\alpha_R}{2q_B}\eta_c\left(\frac{2b_{s_j} - k_{21}c_{s_j}}{\left(1 + k_a a_{s_j} + k_b b_{s_j} + k_c c_{s_j} + k_d d_{s_j}\right)^2}\right)a_{s_j} \tag{12}$$

For Species D (GBL). In the liquid phase

$$\left[d_j - d_{l_{j-1}}\right] = \frac{\alpha_s}{N}\left[d_{l_j} - d_{s_j}\right] \tag{13}$$

and

$$\alpha_s\left[d_{l_j} - d_{s_j}\right] = \frac{\alpha_R}{2q_B}\eta_c\left(\frac{k_{21}c_{s_j} - k_{31}d_{s_j}}{\left(1 + k_a a_{s_j} + k_b b_{s_j} + k_c c_{s_j} + k_d d_{s_j}\right)^2}\right)a_{s_j} \tag{14}$$

For Species E (THF). In the gas phase

$$\frac{de_{g_j}}{dz} = \alpha_E\left[q_{BE}e_{l_j} - e_{g_j}\right] \tag{15}$$

In the liquid phase

$$\int_0^1 \frac{\alpha_E \beta_E}{q_{BE}}\left[q_{BE}e_{l_j} - e_{g_j}\right]dz = \left[e_{l_{j-1}} - e_{l_j}\right] + \alpha_s\left[e_{l_j} - e_{s_j}\right] \tag{16}$$

and

$$\alpha_s\left[e_{l_j} - e_{s_j}\right] = \frac{\alpha_R}{2q_B}\eta_c\left(\frac{k_{31}d_{s_j} - 2k_{41}e_{s_j}}{\left(1 + k_a a_{s_j} + k_b b_{s_j} + k_c c_{s_j} + k_d d_{s_j}\right)^2}\right)a_{s_j} \tag{17}$$

For Species F (n-BuOH). In the liquid phase

$$\left(f_{l_j} - f_{l_{j-1}}\right) = \frac{a_s}{N}\left(f_{s_j} - f_{l_j}\right) \tag{18}$$

and

$$a_s\left(f_{s_j} - f_{l_j}\right) = \eta_c \frac{\alpha_R}{q_B} \frac{k_{41} e_{s_j} a_{s_j}}{\left(1 + k_a a_{s_j} + k_b b_{s_j} + k_c c_{s_j} + k_d d_{s_j}\right)^2} \tag{19}$$

In deriving the energy balance for the nonisothermal BCSR model, the temperature dependence of various key parameters, such as reaction rate constants, reaction equilibrium constants, catalyst effective diffusivity, and saturation solubility, are accounted for. The effective diffusivity was evaluated from the relationship that relates the molecular diffusivity D_m, porosity ϵ, and tortuosity τ

$$D_e(T_0) = D_m \frac{\epsilon}{\tau} \tag{20}$$

Here, the molecular diffusivity D_m was evaluated from the correlation of Wilke and Chang (1955), while the porosity and the tortuosity factors were taken as 0.9 and 3.0, respectively (Chaudhari and Ramachandran, 1980). The solubility of hydrogen in aqueous MAC was experimentally determined (Chaudhari et al., 2002), so the Henry's constant of solubility H_A could be expressed by the following quadratic correlation in solution temperature

$$(H_A)_T = 3.98112 - 0.01582T + 1.575 \times 10^{-5} T^2 \tag{21}$$

where T is the temperature expressed in K and $(H_A)_T$ is the Henry's constant in dimensionless terms. The effect of product concentration on the solubility of hydrogen was assumed to be negligible. The Henry's constant for THF was determined from VLE data (Sada et al., 1975) and was found to be approximately of the order of 1,000 times greater than that of hydrogen

$$(H_E)_T = 155.3 - 0.70247T + 7.875 \times 10^{-4} T^2 \tag{22}$$

The change in the rate and equilibrium constants with respect to temperature can be represented as

$$k_i(T) = k_i(T_0) \exp\left[\frac{E_t}{R_g T_0}\left(1 - \frac{1}{\Theta}\right)\right] \tag{23}$$

$$K_i(T) = K_i(T) \exp\left[\frac{-\Delta H_i}{R_g T_0}\left(1 - \frac{1}{\Theta}\right)\right] \tag{24}$$

The heat evolved during the reaction is assumed to be carried away by the evaporation of the aqueous solvent and THF as well as transfer to the reactor wall, which is characterized by the bed-to-wall heat-transfer coefficient, U_w. Under such conditions where interphase and intraparticle heat-transfer resistances are assumed to be negligible, the energy balance for cell j in the reactor can be expressed in the dimensionless form as

$$\begin{aligned}\left(\Theta_{j-1} - \Theta_j\right) &= \frac{\eta_c \alpha_R \beta 1}{q_B N}\left[\frac{b_{s_j} + 2k_{21} c_{s_j} + 2k_{31} d_{s_j} + k_{41} e_{s_j}}{\left(1 + k_a a_{s_j} + k_b b_{s_j} + k_c c_{s_j} + k_d d_{s_j}\right)^2}\right] a_{s_j} \\ &- \frac{\beta 2}{N}\left(\Theta_j - \Theta_w\right) - (\beta 3)\left(u_{s_{j-1}} - u_{s_j}\right) - (\beta 4)\left(u_{g_{j-1}} - u_{g_j}\right)\end{aligned} \tag{25}$$

The variation in gas velocity has been accounted for as follows

$$u_{g_j} = u_{g_{j-1}} \frac{A_{g_{j-1}}}{A_{g_j}}(1 - X_A) \tag{26}$$

where X_A is the conversion of hydrogen. Any contribution to the gas velocity due to evaporation of THF is assumed to be negligible when compared to hydrogen.

Method of Solution. The solution of the preceding set of nonlinear algebraic equations allows a prediction of the concentrations of all the species and temperature at the exit of each cell as well as the Nth cell (exit of the reactor) for any given set of inlet parameters. In order to express the concentration of the gaseous components H_2 and THF as algebraic equations, Eq. 6 can be integrated to give

$$\frac{a_{g_j} - a_{l_j}}{a_{g_{j-1}} - a_{l_j}} = \exp(-\alpha_A z) \tag{27}$$

By substituting $z = 1/N$, the dimensionless concentration of A in the stream leaving the cell j is

$$a_{g_j} = a_{g_{j-1}} \exp\left(\frac{-\alpha_A}{N}\right) + a_{l_j}\left[1 - \exp\left(\frac{-\alpha_A}{N}\right)\right] \tag{28}$$

Substituting Eq. 27 in Eq. 7 and solving the resulting integral equation gives the following expression for the dimensionless concentration of A in the liquid stream leaving cell j

$$a_{l_j} = \frac{a_{l_{j-1}} + \beta_A\left[1 - \exp\left(\frac{-\alpha_A}{N}\right)\right] a_{g_{j-1}} + \frac{\alpha_s a_{s_j}}{N}}{1 + \beta_A\left[1 - \exp\left(\frac{-\alpha_A}{N}\right)\right] + \frac{\alpha_s}{N}} \tag{29}$$

Once $a_{l,j}$ is known, the concentration of A on the catalyst surface, A_s, can be obtained from Eq. 8. The equations for THF are solved in an analogous fashion. The final expressions of the solution of Eqs. 15 and 16 are

$$e_{g_j} = e_{g_{j-1}} \exp\left(-\frac{\alpha_E}{N}\right) + q_{BE} e_{l_j}\left[1 - \exp\left(-\frac{\alpha_E}{N}\right)\right] \tag{30}$$

$$e_{l_j} = \frac{e_{l_{j-1}} + \frac{\beta_E}{q_{BE}}\left[1 - \exp\left(-\frac{\alpha_E}{N}\right)\right] e_{g_{j-1}} - \frac{\alpha_s e_{s_j}}{N}}{1 + \beta_E\left[1 - \exp\left(-\frac{\alpha_E}{N}\right)\right] - \frac{\alpha_s}{N}} \tag{31}$$

Equations 6 to 19 are combined with Eqs. 25 and 26 and were solved simultaneously using the IMSL nonlinear equation solver (IMSL, MATH/LIBRARY, 1994) to predict the concentrations of the individual species and the temperature at the exit of each cell.

The initial conditions were as follows: At

$$z = 0, \quad a_l = b_l = 1; \quad c_l = d_l = e_l = f_l = 0; \qquad \theta = 1 \quad (32)$$

These conditions imply that the liquid entering the reactor is presaturated with hydrogen and the concentrations of all the products (C, D, E, and F) in the entering liquid stream are zero. For any given set of inlet conditions, the effectiveness factor, the concentration of reactant/product species, and temperature are calculated for the exit of each cell and also for the exit of the reactor. The various dimensionless parameters (mass-transfer parameters, heat-transfer parameters, reaction rate parameters) are calculated from the variables in Table 3. The correlations were selected based on the recommendations by Ramachandran and Chaudhari (1983) and are given in Table 4. The MAC conversion, global rate of hydrogenation, THF productivity, and selectivity to GBL and THF were evaluated. At any given length of the reactor, the fractional conversion of MAC is given as

$$X_B = (1 - b_l) \quad (33)$$

However, since the consumption of aqueous MAC is very rapid, the combined conversion of MAC and SAC is a more useful parameter for assessing the reactor performance. In this case, Eq. 33 becomes

$$X_B = (1 - b_l - c_l) \quad (34)$$

The global rate of hydrogenation (including hydrogen consumption in all the steps) was calculated as

$$R_{H_2} = \tau' \left[C_{l_j} + 2D_{l_j} + 5E_{l_j} + 6F_{l_j} \right] \quad (35)$$

In Eq. 35, τ' is the mean residence time of the liquid in the reactor ($\tau' = u_l/L$), u_l is the liquid velocity, L is the length of the reactor, C_l, D_l, E_l, and F_l are the concentrations of SAC, GBL, THF, and n-BuOH, respectively, at the exit of the reactor. The units for these parameters are presented in the Notation Section. The catalytic effectiveness factor η_c evaluated was found to be >0.97 for all the reaction conditions. This is expected to be so, since the diameter of the catalyst particle was assumed to be 30 microns for all calculations, which indicates negligible intraparticle mass-transfer resistance.

The productivity of THF is defined as follows

$$P_{THF} = \frac{Q_g E_g + Q_l E_l}{V_l} \quad (36)$$

where Q_g is the molar flow rate of gas, E_g is the concentration of THF in the gas phase, and V_l is the reactor volume.

The selectivity to GBL, THF, and n-BuOH is evaluated using the following relationships

$$S_{GBL} = \frac{d_l}{1 - b_l} \times 100 \quad (37)$$

$$S_{THF} = \frac{Q_l E_l + Q_g E_g}{(1 - B_l) Q_l} \times 100 \quad (38)$$

$$S_{\mathrm{BuOH}} = \frac{f_l}{1 - b_l} \times 100 \quad (39)$$

Results and Discussion

In order to understand the effect of various operating parameters on the performance of a BCSR, simulations were performed following the procedure described earlier for the range of conditions typically used in the commercial production for the hydrogenation of maleic acid (Table 5). For any given set of operating and inlet parameters, the corresponding mass-transfer and hydrodynamic parameters were calculated using the correlations given in Table 4. The effect of individual parameters on the conversion of MAC, combined conversion of MAC and SAC, selectivity of SAC, GBL, and THF, global rate of hydrogenation, THF productivity, and temperature rise were calculated. The results are discussed below.

The liquid-phase mixing is an important factor in the performance of a BCSR. This was studied by evaluating the re-

Table 4. Correlations Used for Evaluation of $k_l a_B$, k_s, U_w, and D_m

Parameter	Correlation	Reference
Gas–liquid mass-transfer coefficient	$k_l a_B = 0.6 D_m^{0.5} \left(\frac{\mu_L}{\rho_L} \right)^{-0.12} \left(\frac{S_T}{\rho_L} \right)^{-0.62} d_T^{0.17} g^{0.93} \epsilon_g^{1.1}$	Yoshida and Akita (1965)
Liquid–solid mass-transfer coefficient	$\frac{k_s a_p}{D_m} = 2 + 0.212 \left[\frac{d_p^3 (\rho_p - \rho_L)}{\mu_L D_m} g \right]^{1/3} \left[\frac{d_p u \rho_L}{\mu_L} \right]^{0.112}$	Sano (1974)
Heat-transfer coeficient	$St = 0.1 (ReFrPr^2)^{-0.25} = U_w / \rho_{sl} C_{p,sl} u_g$	Deckwer (1980)
Diffusivity coefficient	$D_m = 7.4 \times 10^{-8} \frac{(\phi M_B)^{\frac{1}{2}} T}{\mu_B V_A^{0.6}}$	Wilke and Chang (1955)

Table 5. Range of Operating Conditions for BCSR Investigated

Catalyst	1% Re–6% Ru/C
Catalyst loading, w	10,100 and 200 kg/m^3, (1%–20% w/w)
Initial concentration of MAC, B_{l_1}	0.862 to 3.448 kmol/m^3, (10%–40% w/w)
H_2 pressure, P	15 MPa
Solvent	Water
Liquid velocity, u_l	2 to 10×10^{-4} m/s
Gas velocity, u_g	2 to 10×10^{-2} m/s
Reactor diameter, D	0.25 m
Total reactor length, L	4 m
Particle diameter, d_p	30 microns
Density of catalyst, ρ_p	2,000 kg/m^3

actor performance for the different number of cells (N) in the mixing-cell model for the same total reactor volume. The results showing the combined conversion of MAC and SAC as a function of the number of cells N are presented in Figures 2a and 2b for different catalyst loadings and liquid velocities. The combined conversion of MAC and SAC was found to increase with an increase in the number of cells and catalyst loading, but to decrease with increasing liquid velocity. The higher conversion for $N = 10$ is consistent with plug-flow conditions. Similar trends with respect to variation in the number of cells, N, were observed when the inlet maleic acid concentration and H_2 pressure were varied. The effect of N on the global rate of hydrogenation and temperature rise (at the exit of the reactor) for different substrate concentrations is shown in Figures 3 and 4. Here again, the global rate of hydrogenation was found to increase with N, with a corresponding increase in the temperature rise. Calculations were also performed to examine the significance of external mass-transfer parameters ($k_l a_B$ and k_s) by varying the gas–liquid and liquid–solid mass transfer coefficients. The values of $k_l a_B$ and k_s were increased and decreased by 10 times, respectively. These showed that for the range of conditions used here, the effect of these parameters was negligible. This suggests that the flow pattern, catalyst loading, intra-particle diffusion, and thermal energy effects will largely influence the reactor performance.

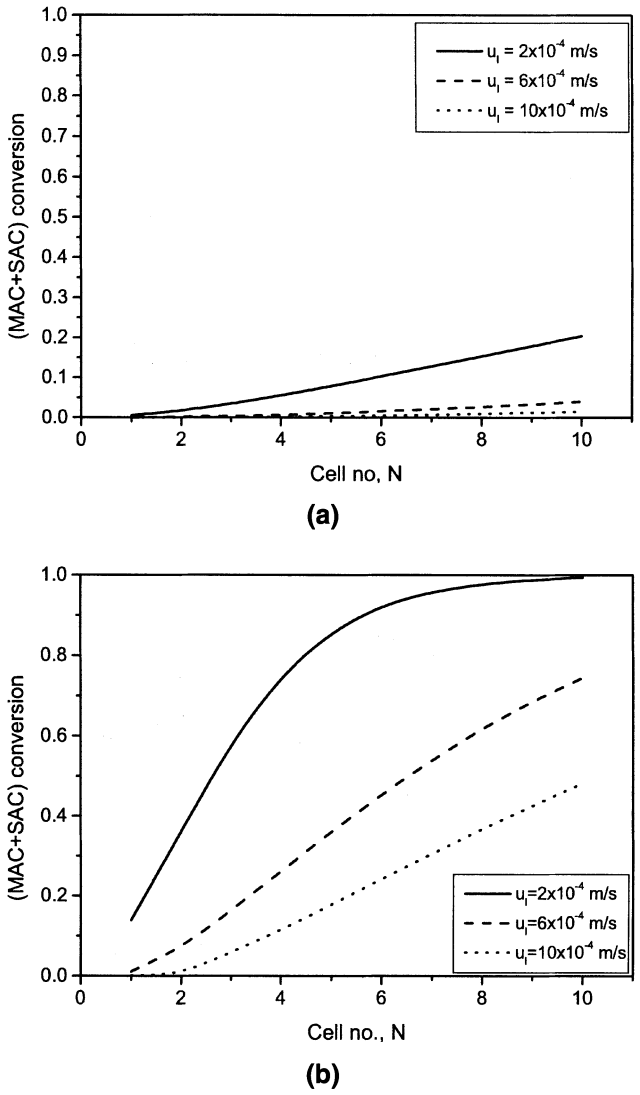

Figure 2. Fractional MAC + SAC conversion along length of the reactor: (a) effect of varying liquid velocity; (b) effect of varying liquid velocity.

Reaction conditions: (a) $w = 10$ kg/m^3, $B_{l_1} = 0.862$ kmol/m^3, $u_g = 6\times10^{-2}$ m/s, $P = 15$ MPa, $T = 523$ K; (b) $w = 100$ kg/m^3, $B_{ij} = 0.862$ kmol/m^3, $u_g = 6\times10^{-2}$ m/s, $P = 15$ MPa, $T = 523$ K).

Effect of catalyst loading

The effect of catalyst loading on the combined conversion of MAC + SAC and the temperature rise at the exit of the reactor is shown in Figures 5 and 6 for different temperatures. The conversion and temperature rise were found to increase with an increase in catalyst loading as well as with an increase in the operating temperature.

Effect of inlet MAC concentration

The effect of inlet MAC concentration on the conversion of MAC + SAC and on the temperature rise at the exit of the reactor is shown in Figures 7 and 8 for different temperatures. The combined conversion of MAC + SAC was found to decrease with an increase in MAC concentration, while the temperature rise was found to increase with MAC concentration at all the temperatures. It must be mentioned here that though the temperature rise at the reactor exit at the inlet temperature of 543 K was only 28 K, the temperature profile shows a maximum temperature rise of 35 K in the intermediate cells (Figure 8b). Thus, for any given set of conditions, a temperature profile exists.

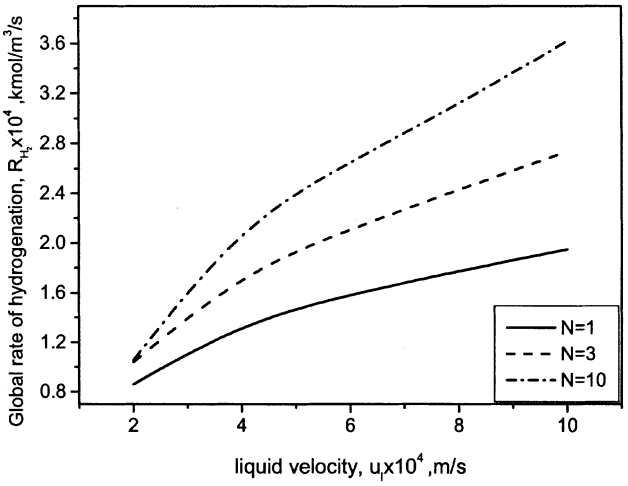

Figure 3a. Global rate of hydrogenation as a function of liquid velocity: effect of mixing.

Reaction conditions: $w = 100$ kg/m^3, $B_{l_1} = 3.448$ kmol/m^3, $u_g = 6 \times 10^{-2}$ m/s, $P = 15$ MPa, $T = 523$ K.

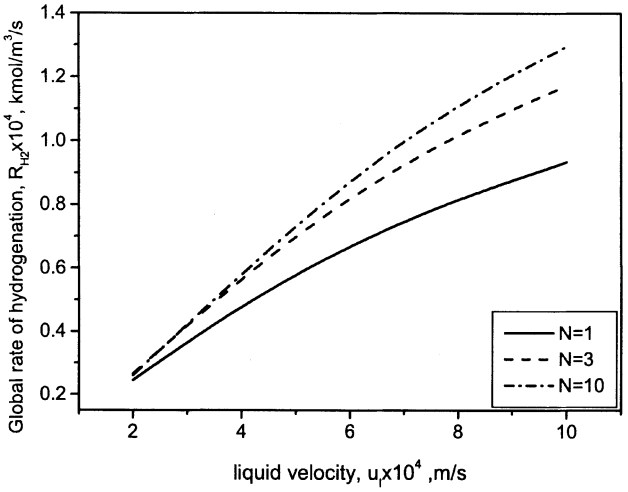

Figure 4a. Global rate of hydrogenation as a function of liquid velocity: effect of mixing for varying substrate concentration.

Reaction conditions: $w = 100$ kg/m^3, $B_{l_1} = 0.862$ kmol/m^3, $u_g = 6 \times 10^{-2}$ m/s, $P = 15$ MPa, $T = 523$ K.

Selectivity behavior

The selectivities to SAC, GBL, and THF were much greater than the selectivity to the minor product *n*-butanol in a BCSR, except at higher catalyst loading and longer residence times. The effect of catalyst loading on the selectivity to SAC, GBL, THF, and *n*-BuOH, and the effect of varying inlet MAC concentration on selectivity to SAC, GBL, THF, and *n*-BuOH are shown in Figures 9 and 10, respectively, for different liquid inlet velocities. It was observed that in both cases, the selectivity of THF was higher for lower liquid velocities. At lower liquid velocities, a high selectivity (up to 80%) can be achieved, which was independent of inlet MAC concentration. The selectivities to GBL, THF, and BuOH as a function of temperature are shown in Figure 11. It was observed that as the temperature increased from 503 K to 543 K, the selectivity to GBL decreased, while the selectivity to THF increased and reached a maximum at $T = 543$ K.

Since removal of volatile THF product by stripping is an important feature of this process, the distribution of THF produced in the gas and liquid phases is important to understand. Figure 12 shows a plot of the ratio of distribution of THF in the gas phase to the total THF produced as a function of gas velocity for different inlet liquid velocities. It was observed that the ratio (THF_{gas}/THF_{total}) increases with an

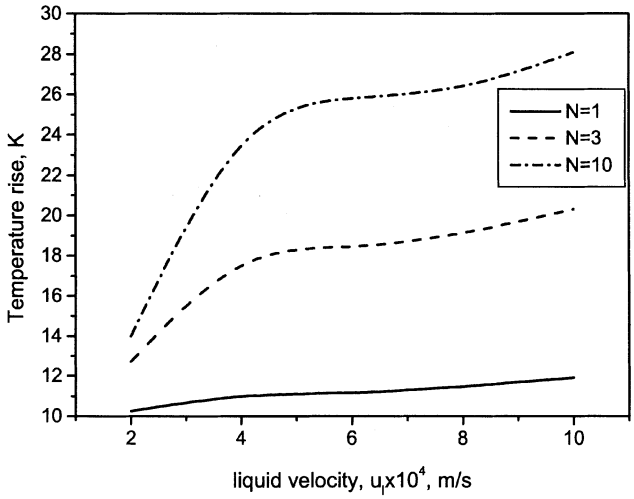

Figure 3b. Temperature rise as a function of liquid velocity: effect of mixing for varying substrate concentration.

Reaction conditions: $w = 100$ kg/m^3, $B_{l_1} = 3.448$ kmol/m^3, $u_g = 6 \times 10^{-2}$ m/s, $P = 15$ MPa, $T = 523$ K.

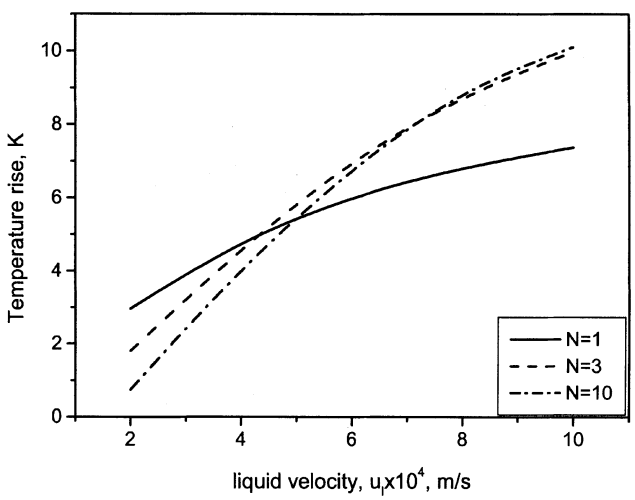

Figure 4b. Temperature rise as a function of liquid velocity: effect of mixing for varying substrate concentration.

Reaction conditions: $w = 100$ kg/m^3, $B_{l_1} = 0.862$ kmol/m^3, $u_g = 6 \times 10^{-2}$ m/s, $P = 15$ MPa, $T = 523$ K.

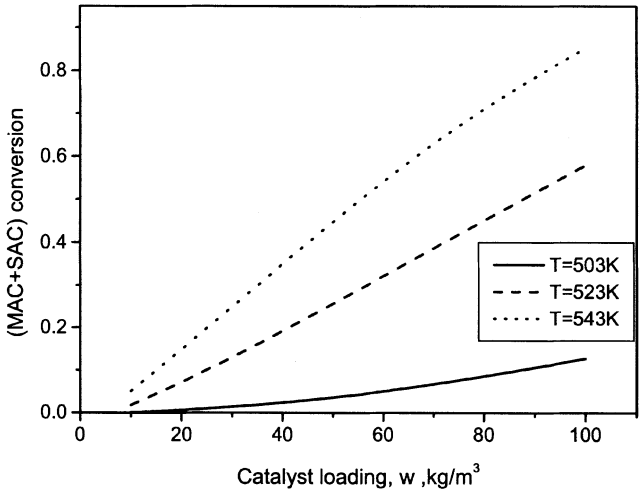

Figure 5. Combined MAC + SAC conversion as a function of catalyst loading: effect of inlet temperature.

Reaction conditions: $B_{l_1} = 0.862$ kmol/m^3, $u_l = 10 \times 10^{-4}$ m/s, $u_g = 6 \times 10^{-2}$ m/s, $P = 15$ MPa, $N = 10$ cells.

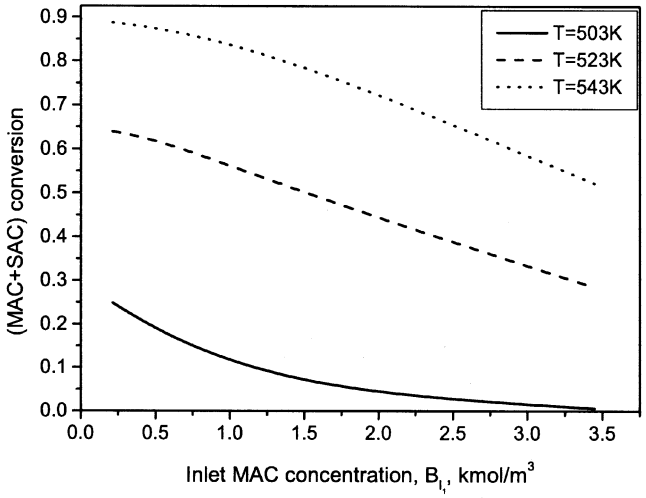

Figure 7. Fractional MAC + SAC conversion as a function of inlet MAC concentration: effect of inlet temperature.

Reaction conditions: $w = 50$ kg/m^3, $u_l = 10 \times 10^{-4}$ m/s, $u_g = 6 \times 10^{-2}$ m/s, $P = 15$ MPa, $N = 10$ cells.

increase in gas velocity; however, it is the highest for lower liquid velocity, that is, a large residence time. The total THF productivity was found to increase with an increase in temperature (Figure 13). The model predictions also indicate that increased selectivity and productivity of THF can be achieved by increasing the catalyst loading, H_2 pressure, reactor inlet temperature, and by using lower liquid velocity or long liquid residence time.

Figure 14 shows the concentration profile of various species along the length of the reactor. As the concentration of MAC approaches to a very low level and the concentration of SAC approaches a maximum, the subsequent hydrogenation reactions are initiated.

In order to understand scale-up effects, calculations were performed for different reactor volumes at fixed L/D ratios to understand the effect of key reaction conditions. As an illustration, Figure 15 shows the THF productivity for catalyst loadings of 25 and 50 kg/m^3. Some interesting trends were observed with respect to THF productivity at different reactor volumes. At $w = 25$ kg/m^3, the THF productivity increases with an increase in reactor volume for all L/D ratios. For $w = 50$ kg/m^3, THF productivity passes through a maximum with a decreasing trend for higher reactor volumes. This is mainly due to the increase in formation of n-BuOH at higher catalyst loadings and longer residence times. The kinetics of n-BuOH formation is not substrate inhibited so that

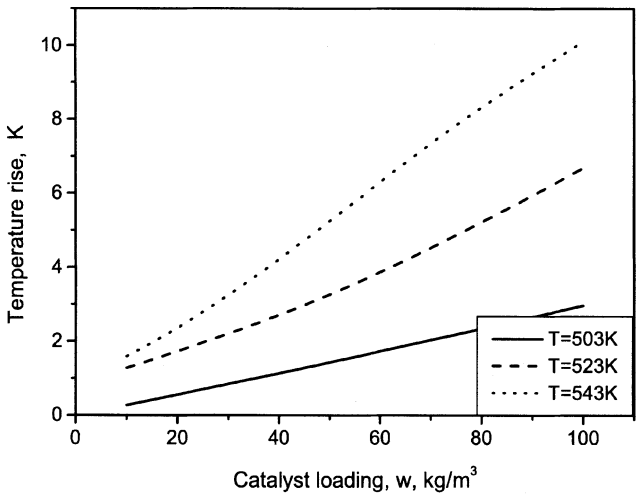

Figure 6. Temperature rise as a function of catalyst loading: effect of inlet temperature.

Reaction conditions: $B_{l_1} = 0.862$ kmol/m^3, $u_l = 10 \times 10^{-4}$ m/s, $u_g = 6 \times 10^{-2}$ m/s, $P = 15$ MPa, $N = 10$ cells.

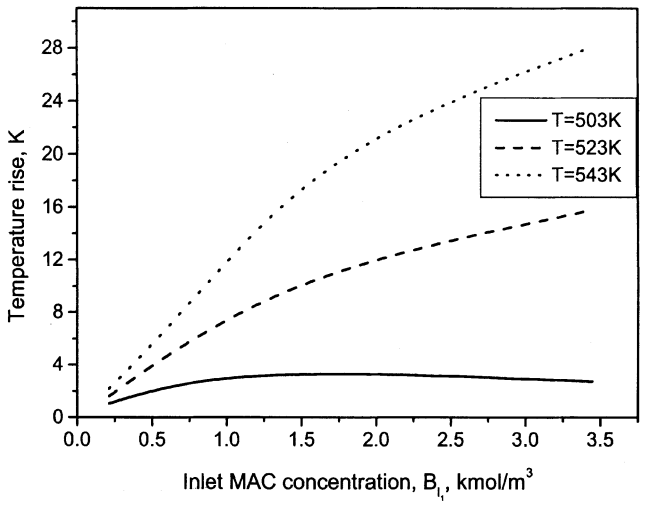

Figure 8a. Temperature rise as a function of inlet MAC concentration: effect of inlet temperature.

Reaction conditions: $w = 50$ kg/m^3, $u_l = 10 \times 10^{-4}$ m/s, $u_g = 6 \times 10^{-2}$ m/s, $P = 15$ MPa, $N = 10$ cells.

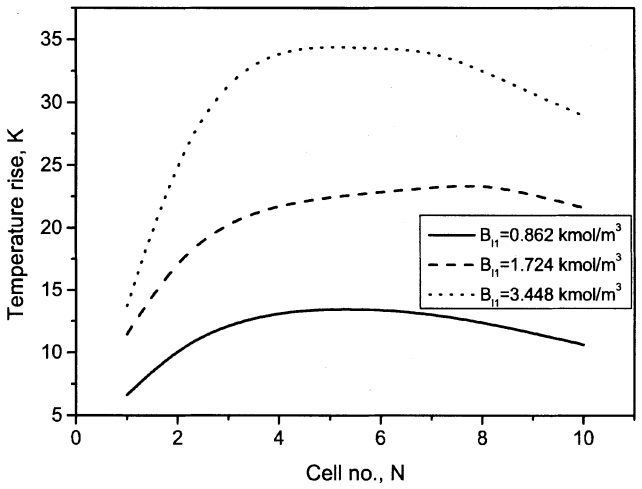

Figure 8b. Temperature profile along the length of the reactor: effect of inlet substrate concentration.

Reaction conditions: $w = 50$ kg/m^3, $u_l = 10 \times 10^{-4}$ m/s, $u_g = 6 \times 10^{-2}$ m/s, $P = 15$ MPa.

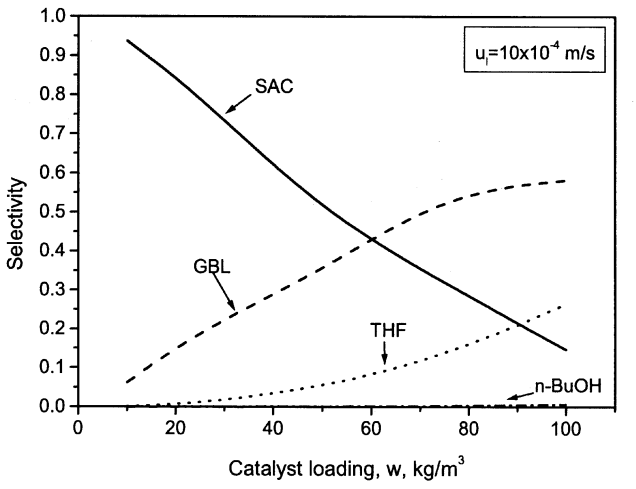

Figure 9b. Selectivity as a function of catalyst loading: effect of liquid velocity.

Reaction conditions: $B_{l_1} = 0.862$ kmol/m^3, $u_l = 10 \times 10^{-4}$ m/s, $u_g = 6 \times 10^{-2}$ m/s, $P = 15$ MPa, $T = 523$ K, $N = 10$ cells.

at higher catalyst loading (where concentrations of SAC and GBL approach nearly zero), the rate of *n*-BuOH formation increases so THF productivity decreases. In this analysis, a fixed value of $N = 10$ has been used (as an illustrative example), which would imply plug flow irrespective of the L/D ratio. However, it does still give some insight into the performance of the reactor with respect to L/D ratio when the mixing pattern remains the same (plug flow in this case).

Comparison of Model Predictions with Experimental Data

The only available data on the Ru–Re/C catalyzed hydrogenation of aqueous MAC appears in a U.S. patent (Schwartz, 1995). These data were used to compare the THF productivity with the model predictions. In one of the patent examples, an experiment in a stirred slurry reactor was reported for the following conditions

$$w = 3 \text{ g in } 150 \text{ mL}, \qquad B_{l_1} = 40\% \text{ (w/w)}, \qquad P = 14 \text{ MPa},$$
$$T = 523\ K, \qquad Q_1 = 20 \text{ cc/h}$$

Under these conditions, a steady-state THF productivity was observed to vary in the range of 1,200–600 STY (space-time yield, g THF/kg catalyst·h) over a period of three weeks. In order to compare these data with the model predictions, calculations were performed for a single cell ($N = 1$) that would

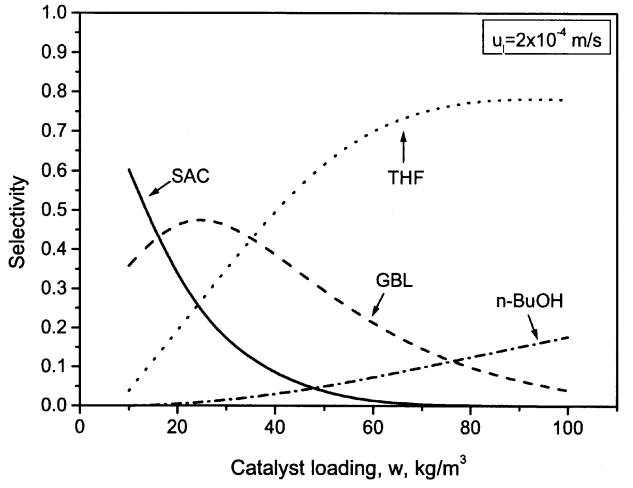

Figure 9a. Selectivity as a function of catalyst loading: effect of liquid velocity.

Reaction conditions: $B_{l_1} = 0.862$ kmol/m^3, $u_l = 2 \times 10^{-4}$ m/s, $u_g = 6 \times 10^{-2}$ m/s, $P = 15$ MPa, $T = 523$ K, $N = 10$ cells.

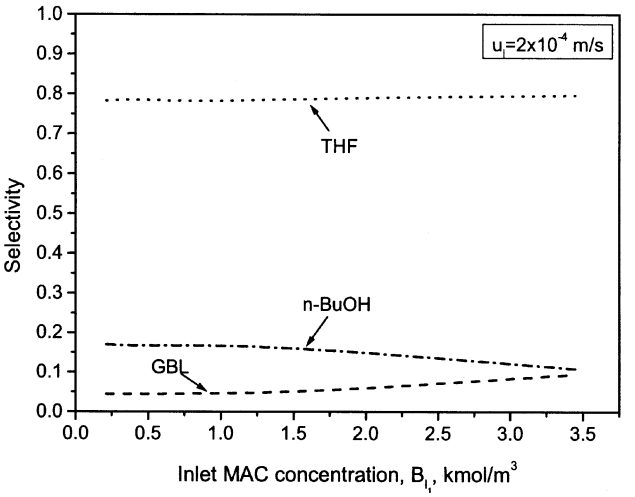

Figure 10a. Selectivity as a function of inlet MAC concentration: effect of liquid velocity.

Reaction conditions: $w = 50$ kg/m^3, $u_l = 2 \times 10^{-4}$ m/s, $u_g = 6 \times 10^{-2}$ m/s, $P = 15$ MPa, $T = 523$ K, $N = 10$ cells.

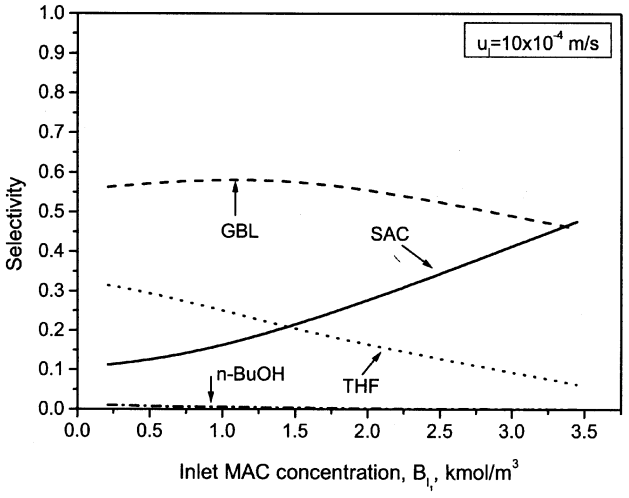

Figure 10b. Selectivity as a function of inlet MAC concentration: effect of liquid velocity.

Reaction conditions: $w = 50$ kg/m^3, $u_l = 10 \times 10^{-4}$ m/s, $u_g = 6 \times 10^{-2}$ m/s, $P = 15$ MPa, $T = 523$ K, $N = 10$ cells.

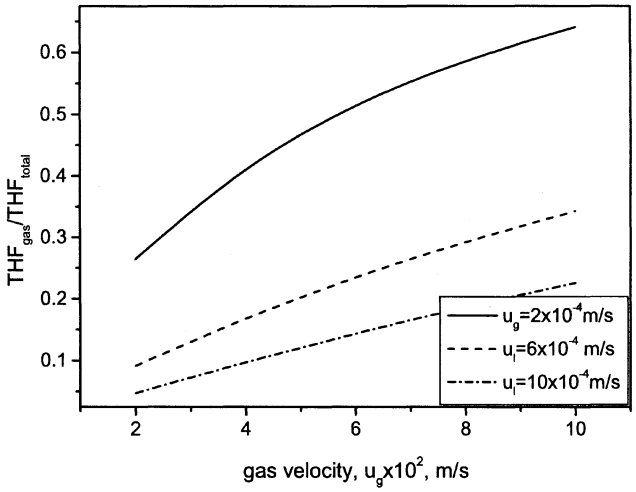

Figure 12. THF distribution as a function of gas velocity: effect of liquid velocity.

Reaction conditions: $w = 50$ kg/m^3, $B_{l_1} = 0.862$ kmol/m^3, $P = 15$ MPa, $T = 543$ K, $N = 10$ cells.

represent a back-mixed stirred slurry reactor. Also, values for the volumetric gas–liquid mass-transfer coefficient, liquid–solid mass-transfer coefficient, and overall heat-transfer coefficient were selected for a stirred slurry reactor from the literature (Bern et al., 1976; Sano et al., 1974; Ramachandran and Chaudhari, 1983). The values of $k_l a_B$, $k_s d_p$, and U_w were calculated as 0.1296 s^{-1}, 1.182×10^{-3} s^{-1}, and 1.108 kJ/Ksm^2, respectively. Since the kinetics used in the model prediction are for a Ru–Re/C catalyst similar to that represented in this patent, it was thought reasonable to at least compare the model predictions with the experimental data in the order-of-magnitude range. For this case, the model predictions showed THF productivity of 700 STY (space-time yield, g THF/kg catalyst·h) and a combined (MAC + SAC) conversion of 90%. The predicted performance is within the range reported in the patent example and suggests the potential utilization of the model for prediction of the reactor performance.

Conclusions

A mixing-cell model for a BCSR has been developed for the hydrogenation of maleic acid solution that incorporates the complex intrinsic reaction kinetics, product volatility, interphase and intraparticle mass-transfer effects, and thermal effects. The variation of the gas velocity due to stripping of volatile product and consumption of gaseous reactant (H_2) has also been accounted for. In each mixing cell, the liquid phase is assumed to be completely back mixed with the gas in plug flow. It is assumed that the catalyst particles are uni-

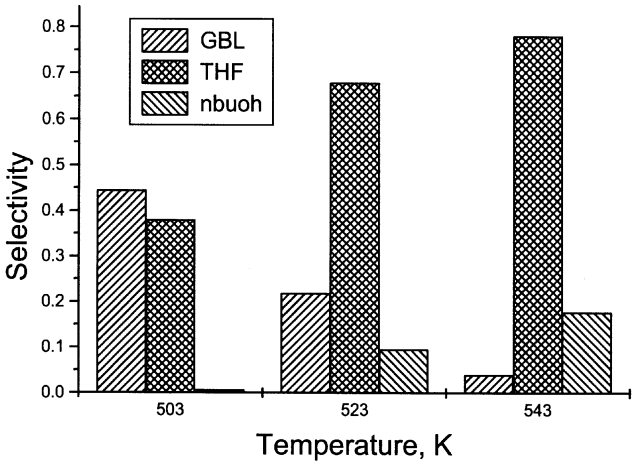

Figure 11. Selectivity as a function of inlet temperature.

Reaction conditions: $w = 100$ kg/m^3, $B_{l_1} = 0.862$ kmol/m^3, $u_g = 6 \times 10^{-2}$ m/s, $u_l = 10 \times 10^{-4}$ m/s, $P = 15$ MPa, $N = 10$ cells.

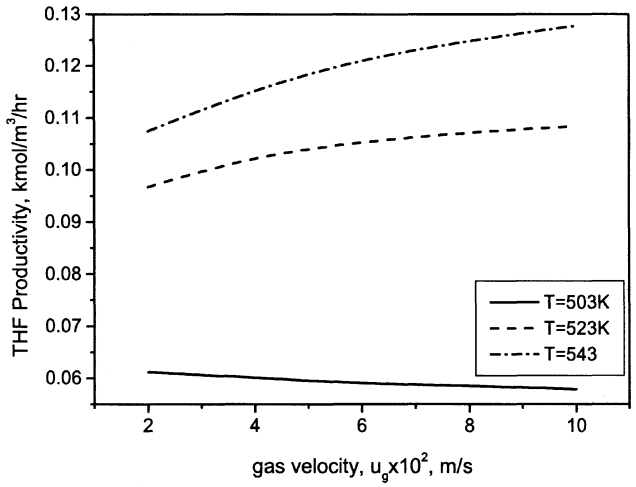

Figure 13. THF productivity as a function of gas velocity: effect of inlet temperature.

Reaction conditions: $w = 100$ kg/m^3, $B_{l_1} = 0.862$ kmol/m^3, $u_l = 10 \times 10^{-4}$ m/s, $P = 15$ MPa, $N = 10$ cells.

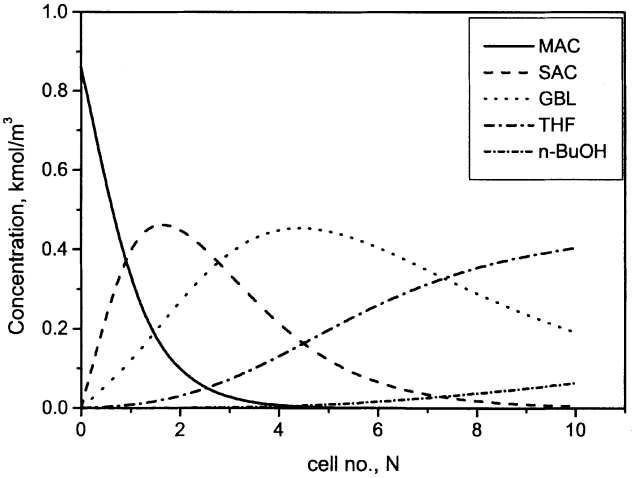

Figure 14. Concentration of various species as a function of reactor length.

Reaction conditions: $w = 100$ kg/m^3, $B_{l_1} = 0.862$ kmol/m^3, $u_l = 10 \times 10^{-4}$ m/s, $u_g = 6 \times 10^{-2}$ m/s, $P = 15$ MPa, $T = 543$ K.

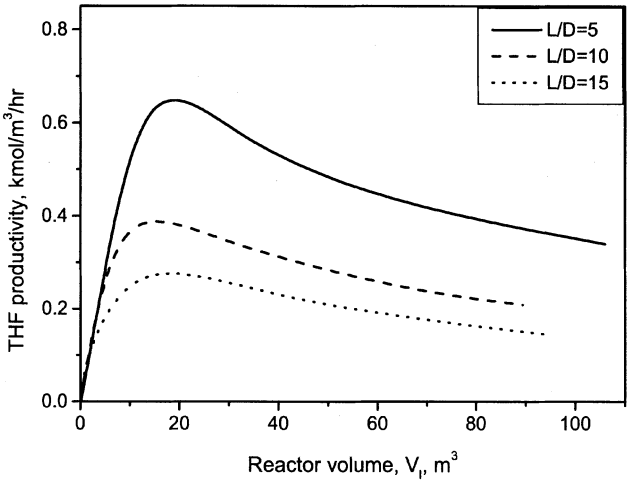

Figure 15b. THF productivity as a function of reactor volume: effect of *L/D* ratio.

Reaction conditions: $w = 50$ kg/m^3, $B_{l_1} = 1.724$ kmol/m^3, $u_g = 8 \times 10^{-2}$ m/s, $u_l = 10 \times 10^{-4}$ m/s, $T = 543$ K, $P = 15$ MPa, $N = 10$ cells.

formly distributed throughout the reactor. This assumption was verified using the criteria proposed by Kato et al. (1972) for catalyst distribution using parameters from the hydrogenation of maleic acid. The reactor model allows a prediction of the reactor performance for any given set of reactor inlet and other process conditions.

The effect of gas and liquid velocity, inlet maleic acid concentration, reactor inlet temperature and catalyst loading on the combined conversion of MAC and SAC, the global rate of hydrogenation, the reactor temperature rise (at the reactor exit), and maximum temperature gradient has been studied. The important observations are:

(1) The combined conversion of MAC and SAC increased with the number of mixing cells, indicating that higher conversion is achieved under plug-flow conditions. However, this effect is significant only at higher catalyst loadings. At lower catalyst loadings, the effect is negligible.

(2) The global rate of hydrogenation was found to increase with an increase in the gas and liquid velocity with a corresponding increase in the reactor temperature.

(3) The productivity of THF increases with an increase in the gas velocity, reactor inlet temperature, and catalyst loading. The relative distribution of THF in the gas phase to the total amount of THF produced (THF_{gas}/THF_{total}) increases with an increase in gas velocity, being the highest at lower liquid velocity.

(4) The THF selectivity was found to increase with an increase in catalyst loading and temperature, but decreases with an increase in liquid velocity.

(5) With an increase in reactor volume, the THF productivity showed an increasing trend at lower catalyst loading. However, at higher catalyst loading, the productivity passed through a maximum due to an increase in *n*-BuOH formation.

The model presented here allows us to evaluate optimum performance for THF productivity. The model proposed here can also be used for the simulation of pilot/commercial-scale performance data as well as the design and scale-up of reactors.

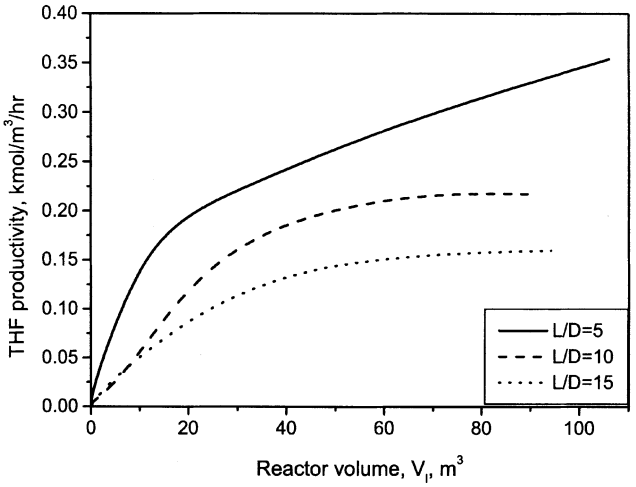

Figure 15a. THF productivity as a function of reactor volume: effect of *L/D* ratio.

Reaction conditions: $w = 25$ kg/m^3, $B_{l_1} = 1.724$ kmol/m^3, $u_g = 8 \times 10^{-2}$ m/s, $u_l = 10 \times 10^{-4}$ m/s, $T = 543$ K, $P = 15$ MPa, $N = 10$ cells.

Notation

a_B = gas–liquid interfacial area, m^2/m^3
a_l = dimensionless concentration of hydrogen in the liquid phase ($A_l \cdot H_A / A_g^0$)
a_B = gas–liquid interfacial area, m^2/m^3
a_p = external surface area of the pellet ($6w/\rho_p d_p$), m^{-1}
A^* = saturation solubility of hydrogen, kmol/m^3
A_l = concentration of hydrogen in the liquid phase, kmol/m^3
A_s = concentration of hydrogen on the catalyst surface, kmol/m^3
b_l = dimensionless concentration of MAC in the liquid phase (B_l/B_{l_1})

B_l = concentration of MAC in the liquid phase, kmol/m^3
B_{l_1} = initial concentration of MAC in the liquid phase, kmol/m^3
b_s = dimensionless concentration of MAC on catalyst surface (B_s/B_{l_1})
c_l = dimensionless concentration of SAC in liquid phase (C_l/B_{l_1})
C_l = concentration of SAC in the liquid phase, kmol/m^3
C_{pl} = heat capacity of liquid, kJ/kg/K
C_{pg} = heat capacity of gas, kJ/kg/K
C_{ps} = heat capacity of water, kJ/kg/K
c_s = dimensionless concentration of SAC on the catalyst surface (C_s/B_{l_1})
D_e = effective diffusivity, m^2/s
D_{ES} = axial dispersion coefficient for solids, m^2/s
D_m = molecular diffusivity, m^2/s
d_p = particle diameter, m
D = reactor diameter, m
d_l = dimensionless concentration of GBL in liquid phase (D_l/B_{l_1})
D_l = concentration of GBL in the liquid phase, kmol/m^3
d_s = dimensionless concentration of GBL on the catalyst surface (D_s/B_{l_1})
e_g = dimensionless concentration of THF in gas phase (E_g/A_g^0)
E_g = concentration of THF in gas phase, kmol/m^3
e_l = dimensionless concentration of THF in liquid phase (E_l/B_{l_1})
E_l = concentration of THF in liquid phase, kmol/m^3
E_i = activation energy for hydrogenation step i, kJ/mol
e_s = dimensionless concentration of THF on the catalyst surface (E_s/B_{l_1})
f_l = dimensionless concentration of n-BuOH in liquid (F_l/B_{l_1})
F_l = concentration of n-BuOH in liquid, kmol/m^3
f_s = dimensionless concentration of n-BuOH on catalyst surface (F_s/B_{l_1})
G = acceleration due to gravity, m/s^2
H_A^1 = Henry's constant of solubility for H_2, kmol/m^3/atm
H_A = dimensionless Henry's constant for H_2 ($1/(H_A^1 \cdot R_g \cdot T)$)
H_E^1 = Henry's constant of solubility for THF, kmol/m^3/atm
H_E = dimensionless Henry's constant for THF ($1/(H_E^1 \cdot R_g \cdot T)$)
k_1 to k_4 = reaction rate constants (m^3/kg)(m^3/kmol)s^{-1}
K_{21} = dimensionless rate constant (k_2/k_1)
K_{31} = dimensionless rate constant (k_3/k_1)
K_{41} = dimensionless rate constant (k_4/k_1)
k_a = dimensionless equilibrium constant ($K_A A_s$)
k_b, k_c, k_d = dimensionless equilibrium constants ($k_b = K_B B_{l_1}$; $k_c = K_C B_{l_1}$; $k_d = K_D B_{l_1}$)
$k_l a_B$ = gas–liquid mass-transfer coefficient, s^{-1}
k_s = liquid–solid mass-transfer coefficient, s^{-1}
K_A, K_B, K_C, K_D = equilibrium constants, m^3/kmol
L = length of reactor, m
q_B = stoichiometric ratio ($B_{l_1}/A_g^0/H_A$)
$q_{B,E}$ = stoichiometric ratio for THF in gas phase ($B_{l_1}/A_g^0/H_E$)
R_1 to r_4 = reaction rates for individual hydrogenation steps (kmol/m^3/s)
R = radius of catalyst particle, m
$(Re)_p$ = particle Reynold's number
R_a = overall rate of hydrogenation, kmol/m^3/s
R_{H_2} = global rate of hydrogenation, kmol/m^3/s
R_g = universal gas constant, kJ/kmol/K
T_0 = inlet temperature, K
T_w = wall temperature, K
U_w = bed-to-wall heat transfer coefficient, kJ/m^2/K/s
u_g = gas velocity, m/s
$u_{s_{i,1}}$ = inlet gas velocity, m/s
u_l = liquid velocity, m/s
$u_{s_{i,1}}$ = inlet solvent velocity, m/s
u_{tp} = terminal settling velocity of particle, m/s
V_l = reactor volume, m^3
w = catalyst loading, kg/m^3
W = average catalyst loading, kg/m^3
Z = dimensionless reactor length

Greek letters

α_A = dimensionless gas–liquid mass-transfer coefficient
α_s = dimensionless liquid–solid mass-transfer coefficient
α_r = dimensionless reaction rate constant
β_A = dimensional parameter ($= u_g H_A/u_l$)
β_E = dimensional parameter ($= u_g H_E/u_l$)
$\beta 1$ = dimensionless thermicity parameter
$\beta 2$ = dimensionless heat-transfer parameter
$\beta 3$ = dimensionless solvent evaporation parameter
$\beta 4$ = dimensionless THF evaporation parameter
$\beta 5$ = dimensionless parameter
ΔH_r = heat of reaction, kJ/mol
ΔH_{ev} = heat of evaporation of water, kJ/kg
$\Delta H_{ev}(THF)$ = heat of evaporation of THF, kJ/kg
ϵ = porosity of the catalyst
η_c = overall catalytic effectiveness factor
θ = dimensionless temperature (T/T_{in})
θ_w = dimensionless wall temperature (T/T_w)
λ_{eff} = effective thermal conductivity, kJ/s·m·°C
ρ_l = density of the liquid, kg/m^3
ρ_g = density of gas, kg/m^3
ρ_p = density of catalyst particle, kg/m^3
τ = tortuosity factor
τ' = residence time, s^{-1}
ϕ = Thiele parameter

Literature Cited

Bern, L., M. Hell, and N. H. Schoon, "Kinetics of the Hydrogenation of Rapeseed Oil. Rate Equations of Chemical Reactions," *J. Amer. Oil Chem. Soc.* **52**, 391 (1975).

Bern, L., J. O. Lidefelt, and N. H. Schoon, "Mass Transfer and Scale up in Fat Hydrogenation," *J. Amer. Oil Chem. Soc.*, **53**, 463 (1976).

Broderick, D. H., and B. C. Gates, "Hydrogenolysis and Hydrogenation of Dibenzothiophene Catalysed by Sulfided CoO-NoO_3/γ-Al_2O_3: The Reaction Kinetics," *AIChE J.*, **27**, 663 (1981).

Brahme, P. H., R. V. Chaudhari, and P. A. Ramachandran, "Modelling of Hydrogenation of Glucose in a Continuous Slurry Reactor," *Ind. Eng. Chem. Proc. Des. Dev.*, **23**, 857 (1984).

Bukur, D. B., "Some Comments on Models for Fischer-Tropsch Reaction in Slurry Bubble Column Reactors," *Chem. Eng. Sci.*, **38**(3), 441 (1983).

Chaudhari, R. V., and P. A. Ramachandran, "Three Phase Slurry Reactors," *AIChE J.*, **26**(2), 177 (1980).

Chaudhari, R. V., C. V. Rode, R. M. Deshpande, R. Jaganathan, T. M. Leib, and P. L. Mills, "Catalysis and Kinetics of Hydrogenation of Maleic Acid in a Batch Slurry Reactor Using a Bimetallic Ru-Re/C Catalyst," *Chem. Eng. Sci.*, **58**, 627 (2003).

Dassori, C. G., "Three Phase Reactor Modeling with Significant Back Mixing in the Liquid Phase Using Modified Cell Model (MCM)," *Chem. Eng. Sci.*, **22**(Suppl.), S679 (1988).

Deckwer, D. W., "On the Mechanism of Heat Transfer in Bubble Column Reactors," *Chem. Eng. Sci.*, **35**(6), 1341 (1980).

Deckwer, W. D., *Bubble Column Reactors*, Wiley, New York (1992).

Ernst, R., and J. Michel, "Hydrogenation Catalyst and Method for Manufacturing Tetrahydrofuran," WO 9202298 (1992).

Govindrao, V. M. H., and M. Chidambaram, "On the Steady State Performance of Cocurrent Bubble Column Slurry Reactors," *Chem. Eng. J.*, **27**, 29 (1983).

Harris, C. K., D. Roekaerts, F. J. J. Rosendal, F. G. K. Buitendijk, A. J. N. Vreenegoor, and H. Wang, "Computational Fluid Dynamics for Chemical Reactor Engineering," *Chem. Eng. Sci.*, **51**(10), 1569 (1996).

IMSL MATH/LIBRARY, *Fortran Subroutine for Mathematical Application*, Vol. 2, Visual Numerics Inc., Houston, TX (1994).
Jaganathan, R., R. V. Gholap, P. H. Brahme, and R. V. Chaudhari, "Performance of a Continuous Bubble Column Slurry Reactor for Hydrogenation of Butynediol," *Proc. ISCRE 2*, Vol. II, India, p. 141 (1987).
Kato, Y., A. Nishiwaki, T. Fakuda and S. Tanaka, "The Behaviour of Suspended Solid Particles and Liquid in Bubble Columns," *J. Chem. Eng. Japan*, **5**, 112 (1972).
Kawakami, K., T. Aio, and K. Kusunoki, "Selectivity of Butadiene Hydrogenation in a Bubble Column Slurry Reactor," *Kagaku Kogaku Ronbunshu*, (in Japanese), **7**(1), 105 (1981).
Kralik, M., J. Ilyavsky, J. Pasek, and P. Lehocky, "Mathematical Dynamic Model of the Continuous Bubble Column Slurry Reactor," *Chem. Eng. Process*, **28**(2), 127 (1990).
Krishna, R., and C. Maretto, "Scale up of a Bubble Column Slurry Reactor for Fischer-Tropsch Synthesis," *Stud. Surf. Sci. Catal. (Natural Gas Conversion V)*, **119**, 197 (1998).
Krishna, R., J. M. van Baten, M. I. Urseanu, and J. Ellenberger, "Design and Scale Up of a Bubble Column Slurry Reactor for Fischer-Tropsch Synthesis," *Chem. Eng. Sci.*, **56**, 537 (2001).
Krishna, R., "A Scale Up Strategy for a Commercial Scale Bubble Column Slurry Reactor for Fischer-Tropsch Synthesis," *Oil Gas Sci. Technol.*, **55**, 359 (2000).
Mathieu, C., E. Dietrich, H. Delmas and J. Jenck, "Hydrogenation of Adiponitrile Catalysed by Raney Nickel: Use of Intrinsic Kinetics to Measure Gas-Liquid Mass Transfer in a Gas Induced Stirred Slurry Reactor," *Chem. Eng. Sci.*, **47**, 2289 (1992).
Mears, D. E., "Tests for Transport Limitations in Experimental Catalytic Reactors," *Ind. Eng. Chem. Proc. Des. Dev.*, **10**, 541 (1971).
Mills, P. L., J. R. Turner, P.A. Ramachandran, and M. P. Dudukovic, "The Fischer-Tropsch Synthesis in Slurry Bubble Column Reactors: Analysis of Reactor Performance using the Axial Dispersion Model," *Top. Chem. Eng.*, **8** (Three-Phase Sparged Reactors), 339 (1996).
Ramachandran, P. A., and J. M. Smith, "Mixing-Cell Model for Design of Trickle-Bed Reactors," *Chem. Eng. Sci.*, **17**, 91 (1979).
Ramachandran, P. A., and R. V. Chaudhari, *Three Phase Catalytic Reactors*, Gorden & Breach, New York (1983).
Sada, E., T. Morisue, and K. Miyahara, "Salt Effects on Vapor-Liquid Equilibrium of Tetrahydrofuran-Water System," *J. Chem. Eng. Data*, **20**, 283 (1975).
Sano, Y., N. Yagamuchi, and T. Adachi, "Mass Transfer Coefficients for Suspended Particles in Agitated Vessels and Bubble Columns," *J. Chem. Eng. Jpn.*, **1**, 255 (1974).
Saxena, S. C., "Bubble Column Reactors and Fischer-Tropsch Synthesis," *Catal. Rev. Sci. Eng.*, **37**(2), 227 (1995).
Schumpe, A., and K. D. P. Nigam, "Mass Transfer in Three-Phase Sparged Reactors," *Top. Chem. Eng.*, **8**, 169 (1996).
Schwartz, J.-A. T., "Ru, Re/Carbon Catalyst for Hydrogenation in Aqueous Solution," U.S. Patent 5,478,952 (1995) (E.I. Du Pont de Nemours and Company).
Shah, Y. T., *Gas-Liquid-Solid Reactor Design*, McGraw-Hill, New York (1979).
Stadig, W., "Three Inventions Combine to Yield New Route to THF. New Technology may Also Find Application in Other Processes," *Chem. Proc.*, **8**, 27 (1992).
Shah, Y. T., B. G. Kelkar, S. P. Godbole, and W. D. Deckwer, "Design Parameters Estimations for Bubble Column Slurry Reactors," *AIChE J.*, **28**(3), 353 (1982).
Wilke, C. R., and P. Chang, "Correlation of Diffusion Coefficients in Dilute Solutions," *AIChE J.*, **1**, 264 (1955).
Yoshida, F., and K. Akita, "Performance of Gas Bubble Columns. Volumetric Liquid Phase Mass Transfer Coefficient and Gas Hold Up," *AIChE J.*, **11**, 9 (1965).

Manuscript received Sept. 30, 2002, and revision received Apr. 3, 2003.